



Publication Year	2018
Acceptance in OA	2020-10-06T13:49:33Z
Title	A census of radio-selected AGNs on the COSMOS field and of their FIR properties
Authors	MAGLIOCCHETTI, MANUELA, Popesso Paola, Brusa Marcella, Salvato Mara
Publisher's version (DOI)	10.1093/mnras/stx2424
Handle	http://hdl.handle.net/20.500.12386/27639
Journal	MONTHLY NOTICES OF THE ROYAL ASTRONOMICAL SOCIETY
Volume	473

A census of radio-selected AGNs on the COSMOS field and of their FIR properties

M. Magliocchetti,^{1★} P. Popesso,² M. Brusa^{3,4} and M. Salvato⁵

¹INAF-IAPS, Via Fosso del Cavaliere 100, I-00133 Roma, Italy

²Excellence Cluster, Boltzmannstr. 2, D-85748 Garching, Germany

³Dipartimento di Fisica e Astronomia, Università di Bologna, Via Gobetti 93/2, I-40129 Bologna, Italy

⁴INAF-Osservatorio Astronomico di Bologna, Via Gobetti 93/3, I-40129 Bologna, Italy

⁵Max Planck Institut für extraterrestrische Physik (MPE), Postfach 1312, D-85741 Garching, Germany

Accepted 2017 September 18. Received 2017 August 1; in original form 2017 March 10

ABSTRACT

We use the new catalogue by Laigle et al. to provide a full census of VLA-COSMOS radio sources. We identify 90 per cent of such sources and sub-divide them into active galactic nuclei (AGNs) and star-forming galaxies on the basis of their radio luminosity. The AGN sample is *complete* with respect to radio selection at all $z \lesssim 3.5$. Out of 704 AGNs, 272 have a counterpart in the *Herschel* maps. By exploiting the better statistics of the new sample, we confirm the results of Magliocchetti et al.: the probability for a radio-selected AGN to be detected at far-infrared (FIR) wavelengths is both a function of radio luminosity and redshift, whereby powerful sources are more likely FIR emitters at earlier epochs. Such an emission is due to star-forming processes within the host galaxy. FIR emitters and non-FIR emitters only differentiate in the $z \lesssim 1$ universe. At higher redshifts, they are indistinguishable from each other, as there is no difference between FIR-emitting AGNs and star-forming galaxies. Lastly, we focus on radio AGNs which show AGN emission at other wavelengths. We find that mid-infrared (MIR) emission is mainly associated with ongoing star formation and with sources which are smaller, younger and more radio luminous than the average parent population. X-ray emitters instead preferentially appear in more massive and older galaxies. We can therefore envisage an evolutionary track whereby the first phase of a radio-active AGN and of its host galaxy is associated with MIR emission, while at later stages the source becomes only active at radio wavelengths and possibly also in the X-ray.

Key words: methods: observational – galaxies: active – galaxies: evolution – galaxies: starburst – infrared: galaxies – radio continuum: galaxies.

1 INTRODUCTION

While in the recent years, there has been a growing interest of the scientific community in extragalactic radio objects, and very ambitious programs like the planned Square Kilometer Array (SKA; Carilli et al. 2004) or its precursors ASKAP (Australian SKA pathfinder; Johnston et al. 2007) and MeerKAT (Jonas 2009) will soon see their first light, investigating the very nature of these sources is not an easy task. They are indeed a mixed bag of astrophysical objects: from the powerful radio-loud Quasi Stellar Objects (QSOs) and Fanaroff Riley II (FRII) (Fanaroff & Riley 1974) galaxies to the weaker Fanaroff Riley I (FRI), low-excitation galaxies and star-forming galaxies, whose contribution to the total radio counts becomes predominant at the sub-mJy level (see e.g. Magliocchetti et al. 2000;

Prandoni et al. 2001; Bonzini et al. 2013, Bonzini et al. 2015; Padovani et al. 2015). Discerning amongst them is only possible via photometric and, whenever possible, spectroscopic follow-ups and to this aim a series of deep-field radio surveys have been performed on very well studied cosmological fields such as COSMOS (Schinnerer et al. 2004; 2007; 2010), GOODS-North (Morrison et al. 2010), VIDEO-XMM3 (McAlpine, Jarvis & Bonfield 2013), VVDS (Bondi et al. 2003), Subaru/XMM (Simpson et al. 2012) and the Extended Chandra Deep Field (Mao et al. 2011 and Bonzini et al. 2012).

Following the launch of the *Spitzer* and *Herschel* satellites, radio sources have also been investigated at mid-infrared (MIR) (e.g. Appleton et al. 2004; Boyle et al. 2007; Magliocchetti, Andreani & Zwaan 2008; Garn, Green & Riley Alexander 2009; Leipski et al. 2009; De Breuck et al. 2010; Norris et al. 2011 amongst the many) and far-infrared (FIR) wavelengths (e.g. Seymour et al. 2011; Del Moro et al. 2013; Magliocchetti et al. 2014, 2016). These studies

* E-mail: manuela@iaps.inaf.it

allowed to probe the sub-population of star-forming galaxies up to $z \sim 3$, and also provided invaluable information on the central engine responsible for radio (and MIR) active galactic nucleus (AGN) emission.

In more detail, Magliocchetti et al. (2014) for the first time investigated the FIR properties of AGNs selected at 1.4 GHz of *all* radio luminosities (except for the ‘monsters’ which do not appear in small and deep fields) and at *all* redshifts $z \lesssim 3.5$. This was done by using the very deep catalogue obtained at 1.4 GHz on the COSMOS field by Schinnerer et al. (2004, 2007, 2010) and Bondi et al. (2008); AGNs were selected solely on the basis of their radio luminosity and FIR information was provided by the PEP survey (Lutz et al. 2011, Lutz 2014). Magliocchetti et al. (2016) then extended this previous analysis to deeper FIR fields such as GOODS-North, GOODS-South and the Lockman Hole.

This work is the third one of the above series and re-analyses the radio and FIR properties of radio-selected sources in the COSMOS field by making use of the very recently published catalogue of redshifts by Laigle et al. (2016). In fact, the COSMOS field (Scoville et al. 2007) covers a large ($\sim 2 \text{ deg}^2$) area and it is observed with very deep ($AB = 25\text{--}26$) multiwavelength data, including imaging in 18 intermediate band filters from Subaru (Taniguchi et al. 2007), which allow to pinpoint emission/absorption lines in the SEDs, and NIR/MIR data from UltraVISTA (McCracken et al. 2012) and IRAC (SPLASH Survey; Capak et al., in preparation). The photometry is homogenized and blending is also taken into account, making the quality of the data, the photometric redshifts and the stellar masses in the Laigle et al. (2016) catalogue among the best available. The availability of reliable photometric redshifts is not limited to normal galaxies but it is also assured for the X-ray sources detected by *Chandra* in a deep and homogeneous manner (Civano et al. 2016; Marchesi et al. 2016).

Indeed, while the work by Magliocchetti et al. (2014) was based on the catalogue by Ilbert et al. (2013), which only provided redshifts for about 65 per cent of the radio sources from the VLA-COSMOS survey, the Laigle et al. (2016) data set provides information for more than 90 per cent of such objects. This is due to the fact that, unlike the Capak et al. (2007) and Ilbert et al. (2010) works which relied on *i*-band selection, the Laigle et al. (2016) catalogue is based on a near-infrared *zYJHK* selection which allows to sample much redder objects and therefore probe higher redshift sources. This extremely high completeness then allows us to reinvestigate the radio and FIR properties of COSMOS radio-selected AGNs and draw conclusions at much higher confidence levels.

Furthermore, galaxies in the Laigle et al. (2016) catalogue are also provided with a flag which indicates whether the source shows signature for AGN emission in a number of wavebands. This information will then be used throughout this work to assess whether there are systematic differences amongst radio-active AGNs which also emit in the MIR or X-ray bands and to envisage an evolutionary connection between these different classes of sources.

Throughout the work, we will assume a Λ CDM cosmology with $H_0 = 70 \text{ km s}^{-1} \text{ Mpc}^{-1}$ ($h = 0.7$), $\Omega_0 = 0.3$, $\Omega_\Lambda = 0.7$ and $\sigma_8^m = 0.8$. Masses for the sources under examination come from the Laigle et al. (2016) catalogue and are calculated using the Bruzual & Charlot (2003) templates and adopting a Salpeter (1955) initial mass function (IMF).

2 THE RADIO-INFRARED MASTER CATALOGUE

The main properties of the radio and FIR catalogues are extensively described in Magliocchetti et al. (2014). Here, we report a brief

summary. The VLA-COSMOS Large Project observed the 2 deg^2 of the COSMOS field at 1.4 GHz (Schinnerer et al. 2004, 2007). The catalogue adopted in our work is that presented in Bondi et al. (2008), which comprises 2382 sources selected above a 1.4 GHz integrated flux of $60 \mu\text{Jy}$.

The COSMOS region has been observed down to $\sim 4 \text{ mJy}$ at $100 \mu\text{m}$ and $\sim 7 \text{ mJy}$ at $160 \mu\text{m}$ by the PACS (Poglitsch et al. 2010) instrument onboard the *Herschel* Space Observatory (Pilbratt et al. 2010) as a part of the PACS Evolutionary Probe (PEP; Lutz et al. 2011) Survey. Infrared counterparts to $F_{1.4 \text{ GHz}} \geq 60 \mu\text{Jy}$ VLA-COSMOS sources have been found by a simple matching technique between the radio and the COSMOS-PEP catalogues. By adopting the same criteria of Magliocchetti et al. (2014), we chose as maximum separation values 4 arcsec at $100 \mu\text{m}$ and 5 arcsec at $160 \mu\text{m}$. We find that 1063 VLA-COSMOS sources (corresponding to 44 per cent of the parent sample) have a counterpart at $100 \mu\text{m}$ and 1100 (corresponding to 46 per cent) have a counterpart at $160 \mu\text{m}$. The total number of $F_{1.4 \text{ GHz}} \geq 60 \mu\text{Jy}$ VLA-COSMOS sources with an infrared counterpart either at $100 \mu\text{m}$ or at $160 \mu\text{m}$ is 1219, corresponding to 51 per cent of the original sample.

Finally, in order to provide the overwhelming majority of radio sources with a redshift determination, in this work we cross-correlated the above sample with the Laigle et al. (2016) catalogue which provides reliable photometric redshifts ($\sigma_{\text{NMAD}} = 0.01$ for galaxies brighter than $I = 22.5$) for COSMOS galaxies, with only a handful of outliers. When possible, we used spectroscopic redshifts available within the COSMOS collaboration.

Given the high positional accuracy of both the radio and the optical–near-infrared surveys, we fix the matching radius to 1 arcsec. This procedure provides redshift estimates for 2123 radio sources (out of which 1199 are spectroscopic), corresponding to ~ 90 per cent of the parent sample. This has to be compared with our previous work where only ~ 65 per cent of the VLA-COSMOS objects were endowed with a redshift determination. Of the 2123 radio sources with redshift of this work, 1173 also have a counterpart on the *Herschel* maps. This corresponds to 96 per cent of FIR-detected galaxies.

3 AGN SELECTION VIA RADIO LUMINOSITY

A tricky point in the process of identifying extragalactic sources observed in monochromatic radio surveys is that of distinguishing between radio emission of AGN origin and that instead due to star-forming processes. The approach we adopt here is that introduced by Magliocchetti et al. (2014) and already used in Magliocchetti et al. (2016). This is based on the results of McAlpine, Jarvis & Bonfield (2013) who provide luminosity functions at 1.4 GHz for the two classes of AGNs and star-forming galaxies. Their results show that the radio luminosity P_{cross} beyond which AGN-powered galaxies become the dominant radio population scales with redshift roughly as

$$\log_{10} P_{\text{cross}}(z) = \log_{10} P_{0,\text{cross}} + z, \quad (1)$$

at least up to $z \sim 1.8$. $P_{0,\text{cross}} = 10^{21.7} [\text{W Hz}^{-1} \text{ sr}^{-1}]$ is the value which is found in the local universe and which roughly coincides with the break in the radio luminosity function of star-forming galaxies (confer Magliocchetti et al. 2002; Mauch & Sadler 2007). Beyond this value, their luminosity function steeply declines, and the contribution of star-forming galaxies to the total radio population is drastically reduced to a negligible percentage (Magliocchetti et al. 2002; Mauch & Sadler 2007).

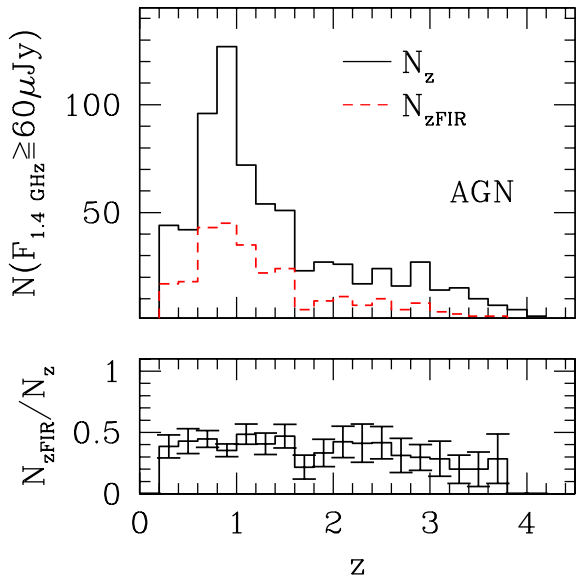


Figure 1. Redshift distribution of COSMOS-VLA radio-selected AGNs with fluxes $F_{1.4\text{GHz}} \geq 0.06$ mJy. The AGN sample is complete up to $z \sim 3.5$. The solid line represents all sources irrespective of their FIR emission, while the dashed line indicates those objects which are also FIR emitters. The bottom panel highlights the ratio between the two quantities. Errorbars correspond to 1σ Poissonian estimates.

We then distinguished between AGN-powered galaxies and star-forming galaxies by means of equation (1) for $z \leq 1.8$ and by fixing $\log_{10} P_{\text{cross}}(z) = 23.5$ [$\text{W Hz}^{-1} \text{sr}^{-1}$] at higher redshifts. This procedure identifies 704 AGNs (corresponding to 33 per cent of the total radio population) and 1419 star-forming galaxies. With respect to our earlier work, these numbers imply an increase of a third of sources in both the AGN and the SF samples and allow us to draw conclusions on the properties of radio-selected sources with and

without an FIR counterpart on much more solid grounds. Also, note that, due to the adopted selection criteria and thanks to the depth of the VLA-COSMOS survey, the AGN samples are *complete* with respect to radio selection at all redshifts $z \lesssim 3.5$, i.e. the considered sample includes *all* radio-emitting AGNs selected at 1.4 GHz in the COSMOS field and endowed with a redshift determination $z \lesssim 3.5$. 272 sources classified as AGNs and 901 sources classified as star-forming galaxies also show up in the *Herschel* maps.

The redshift distribution of radio-selected AGNs is presented in Fig. 1. The filled histogram shows the distribution of all AGNs, independent of their FIR emission, while the dashed (red) histogram represents that of those AGNs which also appear in the *Herschel* maps. The bottom panel highlights the ratio between these two quantities. Errorbars correspond to 1σ Poissonian estimates. As already seen in Magliocchetti et al. (2014), also in the present case we have that the redshift distribution of radio-selected AGNs presents a marked peak at a redshift $z \simeq 1$. However, the better statistics of the present data allow us to identify a prominent tail which extends up to $z \simeq 3.5$ –4 and which in Magliocchetti et al. (2014) only showed up as a secondary peak centred around $z \sim 2.5$. There is no functional difference between the distribution of the parent AGN population and that which corresponds to AGNs with an FIR counterpart. One is the scaled version of the other, and the ratio between these two quantities is roughly constant and equal to the value of ~ 0.5 throughout the whole redshift range probed by our data.

Some more information on the sources under exam can be provided by investigations of the distribution of their radio luminosities, both in the presence and in absence of FIR emission. This is shown in Fig. 2, whereby the left-hand plot shows the distribution of sources at all redshifts, while the one on the right-hand side that of sources divided into redshift intervals. The left-hand plot of Fig. 2 clearly shows that the global distribution of radio-selected AGNs (solid, black line) has a marked peak in the radio luminosity interval $\log_{10} P_{\text{cross}}(z) = 23$ –24 [$\text{W Hz}^{-1} \text{sr}^{-1}$]. Beyond that value,

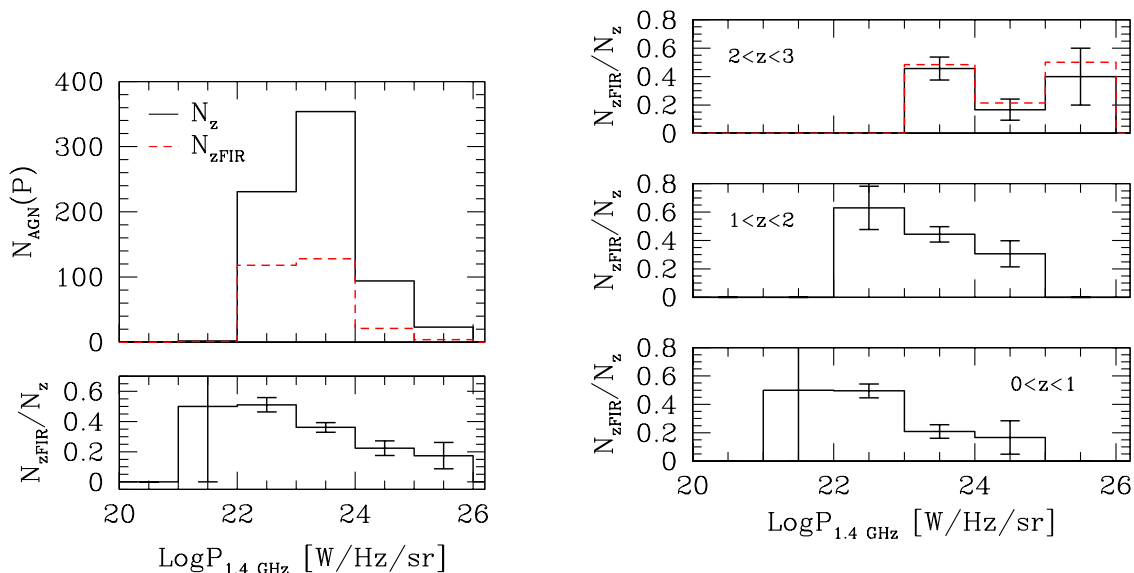


Figure 2. Left-hand panel: distribution of radio powers for $F_{1.4\text{GHz}} \geq 0.06$ mJy COSMOS-VLA radio-selected AGNs. The solid line represents all sources, irrespective of their FIR emission, while the dashed line indicates those objects which are also FIR emitters. The bottom histogram highlights the ratio between the two quantities. Right-hand panel: distribution of the fraction of radio-selected AGNs in the COSMOS-VLA survey which are also FIR emitters as a function of radio luminosity as seen in three different redshift intervals. The dashed histogram in the top panel represents the results obtained if we restrict to sources in the redshift range $z = [2-2.5]$. In both panels, errorbars correspond to 1σ Poissonian estimates.

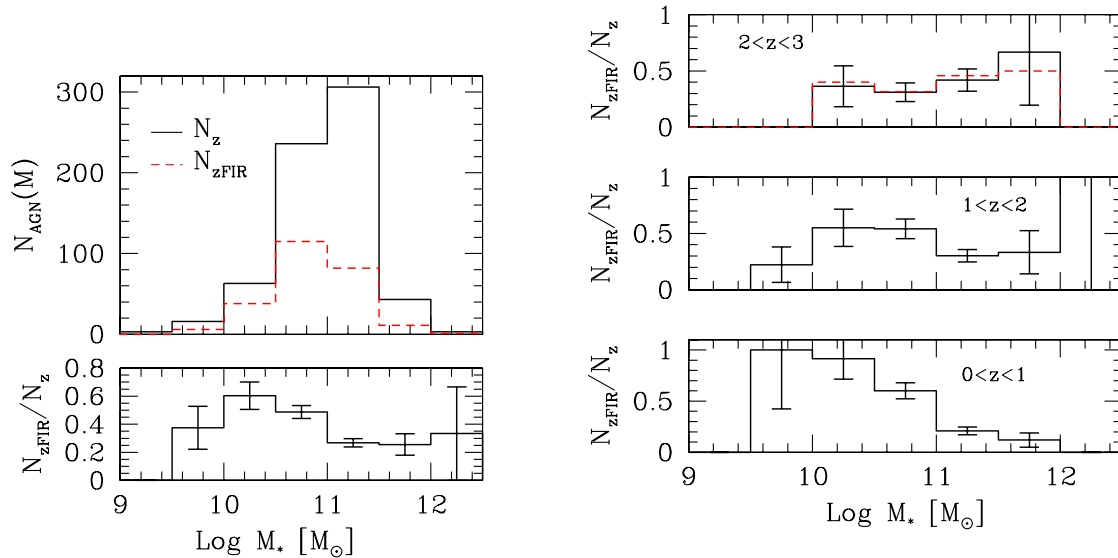


Figure 3. Left-hand panel: distribution of stellar masses for COSMOS-VLA radio-selected AGNs brighter than $F_{1.4\text{GHz}} \geq 0.06$ mJy. The solid line represents all sources irrespective of their FIR emission, while the dashed line indicates those objects which are also FIR emitters. The bottom histogram highlights the ratio between these two quantities. Right-hand panel: distribution of the fraction of radio-selected AGNs in the COSMOS-VLA survey which are also FIR emitters as a function of stellar mass as seen in three different redshift intervals. The dashed histogram in the top panel represents the results obtained if we restrict to sources in the redshift range $z = [2-2.5]$. In both panels, errorbars correspond to 1σ Poissonian estimates.

there is a sharp drop in the number of AGNs of higher luminosities. A very similar drop is also observed in the distribution of radio-selected AGNs which are also associated with FIR emission (red, dashed line). However, the distribution of these sources at lower radio powers does not feature the same sharp peak in the range $\log_{10}P_{\text{cross}}(z) = [22-24]$ [$\text{W Hz}^{-1} \text{sr}^{-1}$]. The net result of these two trends is that the fraction of radio-selected AGNs which also emit at FIR wavelengths (shown in the bottom panel of the left-hand plot) is a strong function of radio luminosity. There is a clear trend which indicates that the number of FIR emitters monotonically decreases with increasing radio luminosity. This decrement is rather significant as the fraction of FIR emitters goes from ~ 60 per cent of the total radio-AGN population at luminosities $\log_{10}P_{\text{cross}}(z) \leq 23$ [$\text{W Hz}^{-1} \text{sr}^{-1}$] down to ~ 20 per cent for luminosities $\log_{10}P_{\text{cross}}(z) \geq 24$ [$\text{W Hz}^{-1} \text{sr}^{-1}$]. However, interestingly enough, the right-hand plot of Fig. 2 clearly shows that this marked decrement is only true in the relatively low ($z \lesssim 2$) redshift universe, and gradually loses its importance when we move from local to more distant sources. Indeed, at higher redshifts, we find that the fraction of FIR emitters is independent of radio luminosity, i.e. that all high-redshift radio-selected AGNs have the same chances of being associated with FIR emission, independent of their radio luminosity. This result confirms those of Magliocchetti et al. (2016), while it partially contradicts that of Magliocchetti et al. (2014) who still found a dependence on radio luminosity also at the highest redshifts, as this was masked by relatively large uncertainties. In this respect, it is worth mentioning that the value of $\sim 0.4-0.5$ found in this work for the fraction of FIR emitters at $z \gtrsim 2$ is determined by the relatively shallow *Herschel* observations on the COSMOS field. Indeed, in the case of deeper observations like those on the two GOODS fields and on the Lockman Hole, one finds that such a percentage reaches the value of 100 per cent (Magliocchetti et al. 2016).

Another interesting feature that can be appreciated in the right-hand plot of Fig. 2 is that the chances for an AGN of a fixed radio luminosity to be an FIR emitter sensibly increase when moving

from the lowest to the highest redshifts probed by our analysis. So, for instance, a source with $P_{1.4\text{GHz}} \simeq 10^{23}$ [$\text{W Hz}^{-1} \text{sr}^{-1}$] will only have an ~ 20 per cent probability of being an FIR emitter at $z \leq 1$, while this percentage rises to ~ 40 per cent in the redshift range $z = [1-2]$, up to ~ 50 per cent for $z = [2-3]$ and a source with $P_{1.4\text{GHz}} \simeq 10^{25}$ [$\text{W Hz}^{-1} \text{sr}^{-1}$] will have a 0 per cent probability of being an FIR emitter both at $z \leq 1$ (zero objects out of one) and $1 \leq z \leq 2$ (zero objects out of 11), while the percentage rises to ~ 40 per cent (4 objects out of 10) at $z = [2-3]$.

This trend, already highlighted by the work of Magliocchetti et al. (2014) and confirmed here on the more solid grounds provided by an almost complete optical identification of all radio-selected AGNs, implies that the probability for a radio-selected AGN to be active in the FIR is both a function of radio power and redshift, whereby powerful sources are more likely to emit at FIR wavelengths at higher redshifts.

Most of the above radio-selected AGNs (696 out of 704) are also endowed with a mass estimate from the Laigle et al. (2016) catalogue.¹ Fig. 3 presents the distribution of such sources as a function of stellar mass. As it was in the previous case, the left-hand plot presents the distribution of masses at all redshifts, while that on the right-hand side illustrates the trends in different redshift intervals. Radio-selected AGNs are on average associated with galaxies with a large stellar mass content. From the left-hand plot of Fig. 3, it is clear that more than 90 per cent of the sources have stellar masses $M_* \geq 10^{10} M_{\odot}$ and more than 50 per cent of them are further associated with galaxies of masses $M_* \geq 10^{11} M_{\odot}$. Those radio-selected AGNs which are also FIR emitters instead present

¹ Note that the masses computed in Laigle et al. (2016) do not include an AGN component in the SED-fitting procedure and are calculated at the photometric redshift values. Both factors could in principle affect their estimates. Further work needs to be developed in order to address this point more properly.

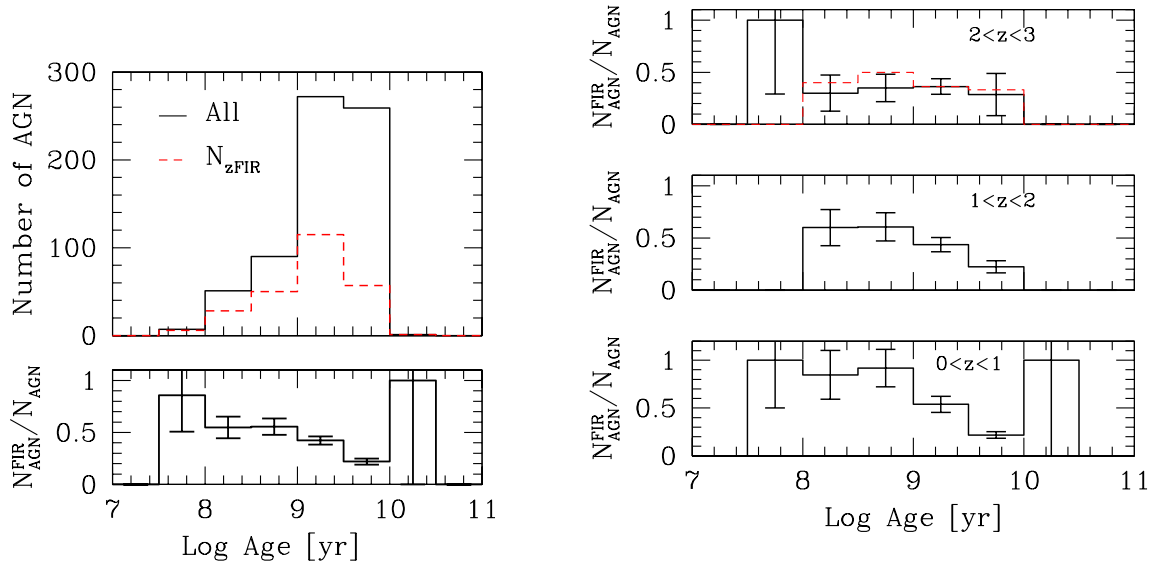


Figure 4. Left-hand panel: distribution of ages for the hosts of COSMOS-VLA radio-selected AGNs brighter than $F_{1.4\text{GHz}} \geq 0.06$ mJy. The solid line represents all sources irrespective of their FIR emission, while the dashed line indicates those objects which are also FIR emitters. The bottom histogram highlights the ratio between these two quantities. Right-hand panel: distribution of the fraction of radio-selected AGNs in the COSMOS-VLA survey which are also FIR emitters as a function of galaxy age as seen in three different redshift intervals. The dashed histogram in the top panel represents the results obtained if we restrict to sources in the redshift range $z = [2-2.5]$. In both panels, errorbars correspond to 1σ Poissonian estimates.

on average slightly lower values for the masses: their distribution (highlighted by the red, dashed line in Fig. 3) peaks between $10^{10.5}$ and $10^{11} M_{\odot}$, rather than in the range $[10^{11}-10^{11.5}] M_{\odot}$ observed in the distribution of the whole radio-AGN population. The net effect of these two different behaviours is that the fraction of radio-selected AGNs associated with FIR emission (represented in the bottom panel of the plot on the left-hand side of Fig. 3) remains roughly constant and equal to the value of 50–60 percent in the relatively low-mass, $M_* \lesssim 10^{11} M_{\odot}$, regime, while it drastically drops to the value of about 20–30 percent for masses higher than the previous value. This implies that FIR emission in radio-selected AGNs is preferentially associated with low-mass objects. However, when do we witness the onset of this trend? The answer to this question can be found in the right-hand plot of Fig. 3 which clearly shows that FIR emitters almost entirely appear in relatively low-mass sources only in the local, $z \lesssim 1$, universe. This phenomenon then loses much of its importance for redshifts $z \gtrsim 1$ and entirely disappears for $z \gtrsim 2$, whereby one finds that all radio-selected AGNs have the same chances of also being FIR emitters independent of the stellar mass associated with their host galaxy.

A trend which is very similar to what observed in the distributions of both radio luminosities and stellar masses of radio-selected AGNs is also found in the distribution of the ages τ of their hosts, which again comes from the work of Laigle et al. (2016). Indeed, in the left-hand panel of Fig. 4, it is possible to appreciate the systematic younger ages of FIR emitters (again represented with the red, dashed line) with respect to the total AGN population: the relative fraction of FIR emitters decreases for ages beyond $\sim 10^9$ yr, and very few of such sources are found for $\tau \gtrsim 10^{9.5}$ yr. But again, as shown in the right-hand panel of Fig. 4, this trend is mostly true in the local, $z \lesssim 1$, universe, while it starts losing its importance at higher redshifts and by $z \simeq 2$ there are no appreciable differences between the ages of radio AGNs which are also FIR emitters and those of the whole radio-AGN population.

As a caveat, we stress that the results presented in the top right-hand panels of Figs 2–4 were obtained for sources up to $z = 3$. However, we note that the McAlpine, Jarvis & Bonfield (2013) data on which our selection method is based only extends to $z = 2.5$. To make sure our results are not biased by an incorrect extrapolation to higher redshifts, we have then re-calculated all the previous quantities for sources in the redshift range $z = [2-2.5]$. These are represented in the top right-hand panels of Figs 2–4 by the dashed histograms. As it is possible to appreciate, the distributions in the two $z = [2-3]$ and $z = [2-2.5]$ intervals are virtually identical. This, together with the fact that very little evolution is observed in the AGN luminosity function of McAlpine, Jarvis & Bonfield (2013) in the whole $z = [1.8-2.5]$ redshift range, gives us confidence that the extrapolation performed to select radio-emitting AGNs for $z \geq 2.5$ is a sensible one.

Also, we made sure that contamination from star-forming galaxies to the AGN sample in the proximity of P_{cross} did not affect our results and conclusions. To this aim, we have recalculated all the quantities presented in Figs 2–4 for a smaller AGN subset obtained by considering only those 444 sources with $P(z) > P^*(z) \equiv 2 \times P_{\text{cross}}(z)$. The choice for such a new luminosity threshold ensures that the possible fraction of contaminants is now drastically reduced to a very negligible quantity at all redshifts (confer the appendix). While, by construction, this selection reduces the number of low-luminosity AGNs and therefore of high-redshift sources, no other difference is observed in any of the distributions presented in this section. Therefore, we can safely conclude that possible contamination of the AGN sample at the lowest radio luminosities due to the presence of unremoved star-forming galaxies is not expected to affect any of our conclusions which can be summarized as: FIR emitters differentiate from the whole population of radio-selected AGNs only in the local, $z \lesssim 1$, universe. At higher redshifts, there is no difference between the properties of FIR-active and FIR-inactive sources and these two classes are indistinguishable one from the other.

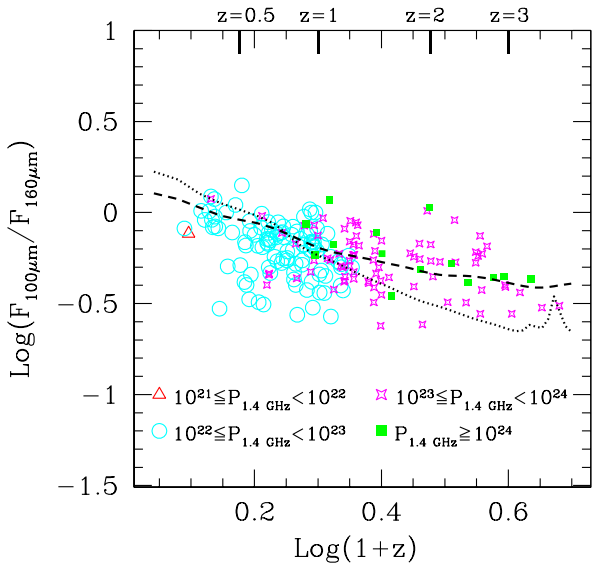


Figure 5. Ratio between $F_{100\mu\text{m}}$ and $F_{160\mu\text{m}}$ fluxes as a function of redshift for radio-selected AGNs with an FIR counterpart from the PEP survey. Different symbols correspond to different intervals for the radio luminosity (measured in $\text{W Hz}^{-1} \text{sr}^{-1}$). The dashed line represents the trend obtained for the SED of M82, while the dotted one corresponds to Arp220 (see the text for details).

4 FIR PROPERTIES

Magliocchetti et al. (2014, 2016) have shown that FIR emission from the hosts of radio-active AGNs is entirely to be attributed to star-forming processes within the galaxy itself. This is also true in the present case. In fact, as Fig. 5 clearly illustrates, except for a very few outliers, the FIR colours of radio-selected AGNs of all luminosities and at all redshifts all lie on the curves identified by the spectral energy distributions (SEDs) of two standard star-forming galaxies: M82 (dashed line) and Arp220 (dotted line). Despite this finding, in

the majority of cases the flux ratios $q_{100} = \log_{10} [F_{100\mu\text{m}}/F_{1.4\text{GHz}}]$ and $q_{160} = \log_{10} [F_{160\mu\text{m}}/F_{1.4\text{GHz}}]$ of these sources indicate an excess of radio activity with respect to that produced by ‘pure’ star-forming processes, most likely to be attributed to the presence of a central, radio-emitting, AGN. This is seen in both panels of Fig. 6 which illustrate the distribution of the quantities q_{100} (left-hand plot) and q_{160} (right-hand plot) as a function of redshift for radio-selected AGNs of different radio luminosities, once again compared with the SEDs obtained for M82 and Arp220.

Some interesting insights on the mechanisms which regulate star formation in radio-selected AGNs can be obtained from a comparison of the FIR properties of this class of objects with those exhibited by the population of star-forming galaxies, where once again this latter class has been selected from the Bondi et al. (2008) catalogue by following the method highlighted in Section 3. To this aim, we have calculated the bolometric luminosities L_{FIR} of both populations by integrating over the whole 8–1000 μm range chosen templates of star-forming galaxies which best fitted the FIR data and subsequently extrapolated their star formation rates (SFRs) according to the standard relation (Kennicutt 1998, which holds for a Salpeter IMF and for stellar masses in the range $\sim 0.1\text{--}100 M_{\odot}$): $\text{SFR} [M_{\odot} \text{yr}^{-1}] = 1.8 \times 10^{-10} L_{\text{FIR}}/L_{\odot}$.

The distribution of L_{FIR} for both classes of sources is presented in Fig. 7, whereby star-forming galaxies are represented by the filled red histogram, while the blue dashed one is for AGNs. First of all, our data clearly show that radio-active AGNs are extremely luminous sources. Their distribution peaks at around $10^{12.5} L_{\odot}$ and presents a tail of sources as bright as $\sim 10^{14} L_{\odot}$. Also, radio-selected AGNs are on average brighter than star-forming galaxies selected from the same radio sample. Indeed, these latter objects present a distribution which peaks at lower, $L_{\text{FIR}} = [10^{11}\text{--}10^{12}] L_{\odot}$, luminosities and there are practically no sources with L_{FIR} beyond $10^{13} L_{\odot}$. This is better seen in the bottom panel of Fig. 7 which shows the relative weight of the two populations of radio-selected sources as a function of FIR luminosity. The fraction of AGNs drastically increases for $L_{\text{FIR}} \gtrsim 10^{11.5} L_{\odot}$, and they become the dominant population in sources brighter than $\sim 10^{13} L_{\odot}$. We note that such

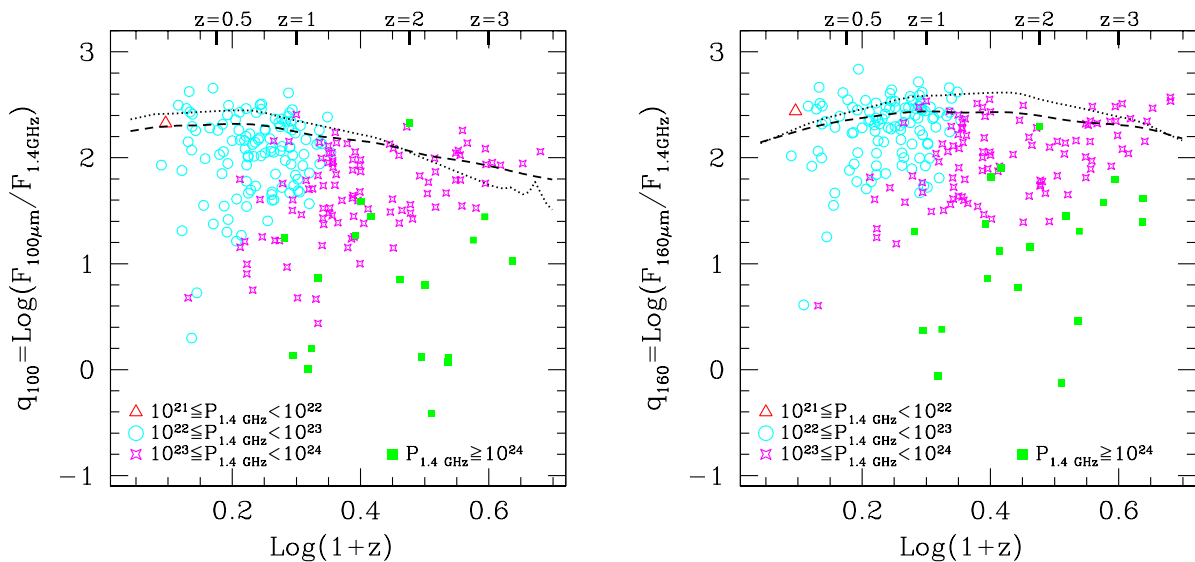


Figure 6. Ratio between $F_{100\mu\text{m}}$ and $F_{1.4\text{GHz}}$ fluxes (left-hand panel) and $F_{160\mu\text{m}}$ and $F_{1.4\text{GHz}}$ fluxes (right-hand panel) as a function of redshift for radio-selected AGNs with an FIR counterpart from the PEP survey. Different symbols correspond to different intervals for the radio luminosity (measured in $\text{W Hz}^{-1} \text{sr}^{-1}$). The dashed lines represent the trends obtained for the SED of M82, while the dotted ones correspond to Arp220 (see the text for details).

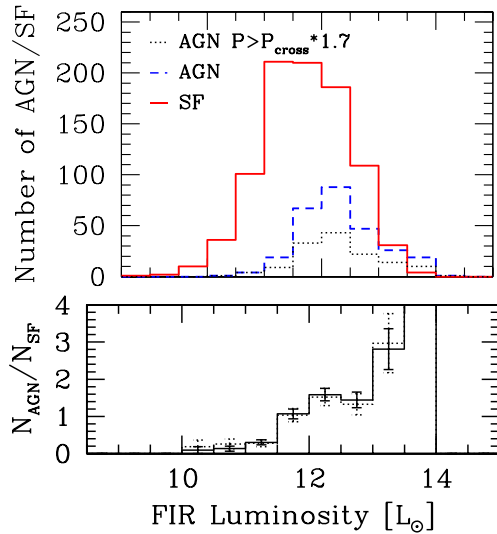


Figure 7. Distribution of FIR luminosities for radio-selected AGNs (blue, dashed line) and radio-selected star-forming galaxies (red, solid line) with a counterpart in the PEP maps. The dotted histogram indicates the luminosity distribution of radio-selected AGNs with radio luminosities $\log_{10} P = \log_{10} P_{\text{cross}} + 0.2$. The bottom panel represents the ratio between these three quantities: AGN/SF (solid line) and AGN with $\log_{10} P = \log_{10} P_{\text{cross}} + 0.2$ over SF (dotted line). These are all appropriately rescaled for the total number of sources in the considered catalogues. Errorbars correspond to 1σ Poissonian estimates.

a finding is robust with respect to possible contaminations of the AGN sample. In fact, if we concentrate on a smaller subset obtained by only considering radio-selected AGNs with luminosities brighter than $P(z) = 2 \times P_{\text{cross}}(z)$, we obtain the very same trend (confer dotted histogram in the bottom panel of Fig. 7), despite having used roughly half of the available sources.

The above result implies that the presence of a radio-active AGN within a galaxy does not inhibit its star formation activity but, on the contrary, that such an activity is probably favoured by the very same presence of the central AGNs. In other words, what we are witnessing is the likely presence of positive feedback, possibly due to the winds produced by the radio-active AGNs which boost star formation within its host. This issue will be better discussed in Section 5.

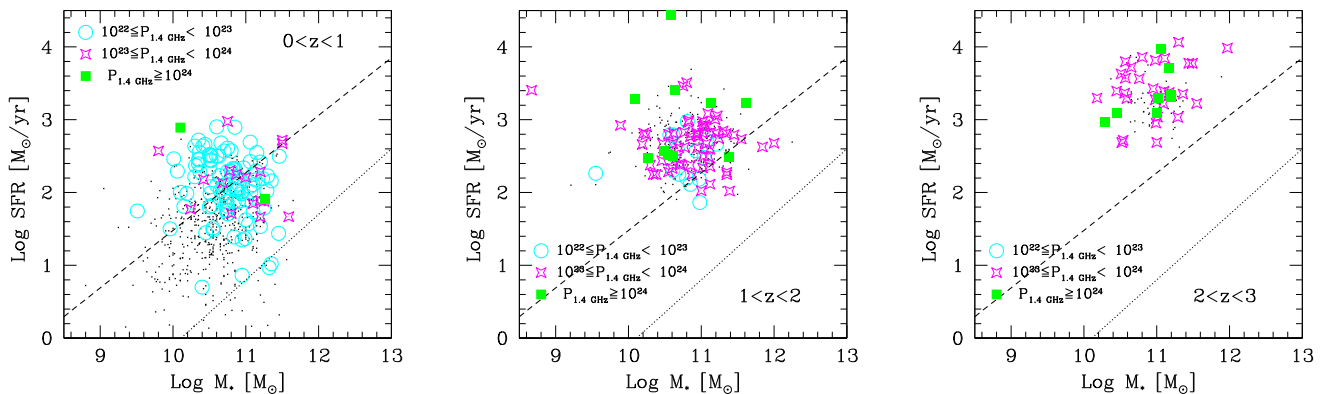


Figure 8. SFRs as a function of stellar mass for radio-selected AGNs in three different redshift intervals. Sources are colour coded according to their radio luminosity (expressed in $[\text{W Hz}^{-1} \text{sr}^{-1}]$ units). Black dots indicate the distribution observed for radio-selected star-forming galaxies of all radio luminosities. The dashed lines indicate the relation obtained for main-sequence galaxies at $z \sim 2$ by Rodighiero et al. (2011), while the dotted lines that derived for local galaxies by Brinchmann et al. (2004) and Peng et al. (2010).

Some more differences between the two populations of radio-selected AGNs and star-forming galaxies can be appreciated by investigating the distributions of their SFRs and specific star formation rates (SSFR, defined as SFR over stellar mass) as a function of stellar mass. This is done in Figs 8 and 9, where the three panels within each figure refer to different redshift ranges. In both figures, star-forming galaxies of all radio luminosities are represented as black dots, while FIR-emitting AGNs are colour coded according to their radio power. In order to guide the eye, the dashed and dotted lines in Fig. 8, respectively, indicate the relation obtained for main-sequence galaxies at $z \sim 2$ by Rodighiero et al. (2011) and that derived for local galaxies by Brinchmann et al. (2004) and Peng et al. (2010). What is clearly visible from both figures is that, independent of their radio power, FIR-active AGNs and star-forming galaxies are indistinguishable from each other at all redshifts beyond $z \simeq 1$. Indeed, they present the very same distribution of stellar masses, star-forming rates and consequently of specific star-forming rates. In the local universe though this similarity breaks down and the two populations exhibit different properties: AGNs tend to be more massive and, most of all, more FIR-bright than star-forming galaxies. The SFRs of this latter population can be as low as ~ 0 and do not extend further than $\sim 10^2 M_{\odot} \text{yr}^{-1}$. On the other hand, irrespective of their radio luminosity, FIR-emitting AGNs are basically only found above SFRs $\simeq 30 M_{\odot} \text{yr}^{-1}$ and can present SFRs as high as $10^3 M_{\odot} \text{yr}^{-1}$. Indeed, radio-selected star-forming galaxies and AGNs at $z \lesssim 1$ occupy two well-defined portions of the SSFR–mass plane (confer left-hand panel of Fig. 9), with very little superposition between the two populations.

These results are in agreement and extend the findings of the former sections which indicate that for redshifts above ~ 1 there is very little or even no difference between radio-selected AGNs and the sub-population of those which are also active at FIR wavelengths. Here, we have seen that, at the same high redshifts, there is also no difference between FIR-active, radio-selected AGNs and FIR-active, radio-selected star-forming galaxies. In all cases, differences only appear in the local universe: radio-active AGNs progressively start becoming FIR-quiet, the more as the higher are their radio luminosities and the mass and age of their hosts, so that FIR activity remains preferentially locked in galaxies which are smaller and younger than the average parent population (confer Section 3). At the same time, AGNs are found associated with hosts of masses which are also higher than those characterizing

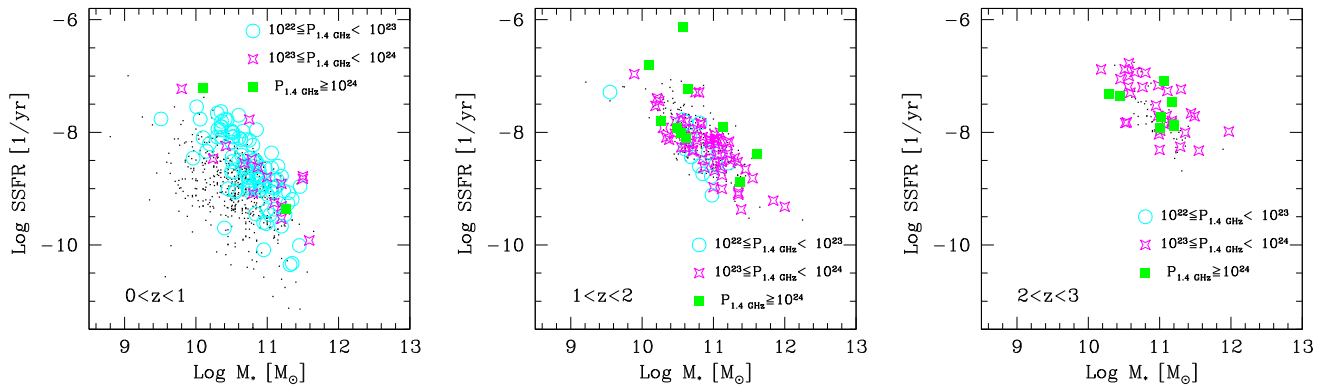


Figure 9. SSFRs as a function of stellar mass for radio-selected AGNs in three different redshift intervals. Sources are colour coded according to their radio luminosity (expressed in $[W \text{ Hz}^{-1} \text{ sr}^{-1}]$ units). Black dots indicate the distribution observed for radio-selected star-forming galaxies of all radio luminosities.

Table 1. Number of radio-selected AGNs with fluxes $F_{1.4\text{GHz}} \geq 0.06$ mJy as taken from the COSMOS-VLA survey. The first row refers to the whole sample, the second one to those which also show AGN emission in the MIR band, while the third row is for sources which are also identified as AGNs in the X-ray band. N_{TOT} refers to the total number of AGNs, while N_{FIR} indicates the number of objects which are also detected at FIR wavelengths. The percentage symbols indicate the percentage of radio-selected AGNs which are also detected at the different wavebands considered in our work. In the second column, we report those for all sources, while the fourth column indicates those for radio-selected AGNs which also emit in the FIR.

	N_{TOT}	per cent	N_{FIR}	per cent
Parent sample	704	–	272	–
MIR detected	141	20.0	83	30.5
X-ray detected	182	25.8	81	29.8

star-forming galaxies, and the few AGNs which still emit at FIR wavelengths in the local universe on average exhibit much higher FIR luminosities (and consequently star-forming rates) than sources undergoing a pure process of stellar formation (confer left-hand panels of Figs 8 and 9).

5 RADIO-SELECTED AGNS OF DIFFERENT NATURE

Galaxies in the COSMOS catalogue provided by Laigle et al. (2016) are also flagged according to whether they present signatures of AGN activity in their spectra or SEDs. This is then also true for the radio-selected AGNs considered in this work. We therefore looked for flags in order to determine whether our sources were also identified as AGNs in the X-ray or MIR bands. We stress that we had to limit our analysis only to these two sub-populations as, unlike the products of X-ray and MIR selection, optically identified AGNs do not belong to a homogeneous sample, therefore no statistical information could be drawn from these objects.

X-ray information comes from the *Chandra COSMOS-Legacy Survey* (Civano et al. 2016; Marchesi et al. 2016) which includes X-ray sources down to a flux limit $f_X = 2 \times 10^{-16} \text{ erg s}^{-1} \text{ cm}^{-2}$ in the 0.5–2 KeV band. MIR selection is instead based on the power-law behaviour in the MIR/*Spitzer*-IRAC bands of the SEDs of the considered sources (Donley et al. 2012; Chang et al. 2017).

The results of our cross-match are summarized in Table 1. Between 20 and 26 per cent of radio-emitting AGNs are also identified as AGNs in the MIR or X-ray band, respectively. This figure rises up

to ~ 30 per cent in the case of MIR AGNs which are also detected at FIR wavelengths, while it basically stays constant in the case of X-ray-emitting AGNs. These findings imply a mild preference for radio-selected AGNs which also emit in the MIR to appear in sources associated with stellar production, while X-ray emission of AGN origin seems to be roughly independent of the FIR activity of its host galaxy.

With the above information at hand, we can investigate the very nature of radio-active AGNs and determine whether there is any substantial difference between those which are only active at radio wavelengths and those which also emit in other parts of the spectrum.

First of all, as shown in Fig. 10 and with the possible exception of the highest luminosity regime probed by our analysis, there is a hint that, while the chances for a radio-active AGN to also be an X-ray emitter seem to be independent of its radio luminosity, this is not true for AGNs which instead also emit in the MIR band, as the probability for MIR emission seems to be monotonically enhanced in radio-selected AGNs of higher and higher radio luminosity.

A similar behaviour is also observed in the distribution of the stellar masses of the hosts of radio-selected AGNs (confer Fig. 11). In fact, even in this case, we observe a substantial consistency of the relative fraction of X-ray emitters with stellar mass, while there is a clear trend for radio-active AGNs which also emit in the MIR to preferentially reside in galaxies of smaller masses. At the same time, radio-selected AGNs which are also X-ray emitters show the same distribution of ages τ as the parent radio-AGN population, while those radio AGNs which also emit in the MIR are found to be associated with systematically younger galaxies (confer Fig. 12).

The above comparisons highlight an interesting fact: the sub-population of radio-selected AGNs which also emit in the X-ray constitutes a class of sources which is indistinguishable from its parent population in terms of radio luminosity and also of stellar masses and ages of their host galaxies. There is neither a preferential level of radio activity of the central black hole nor a preferential sub-galaxy environment which can determine whether the radio-active AGNs will also emit in the X-ray band or not. On the contrary, MIR emission of AGN origin in radio-selected AGNs seems to be favoured in sources which are radio-bright and hosted by galaxies which are relatively small and young.

This effect is better visible in Fig. 13 which shows the distribution of stellar masses and ages for the hosts of radio-selected AGNs which are also active in the MIR (green squares) and X-ray (red circles) bands: AGNs which are also active in the X-ray are

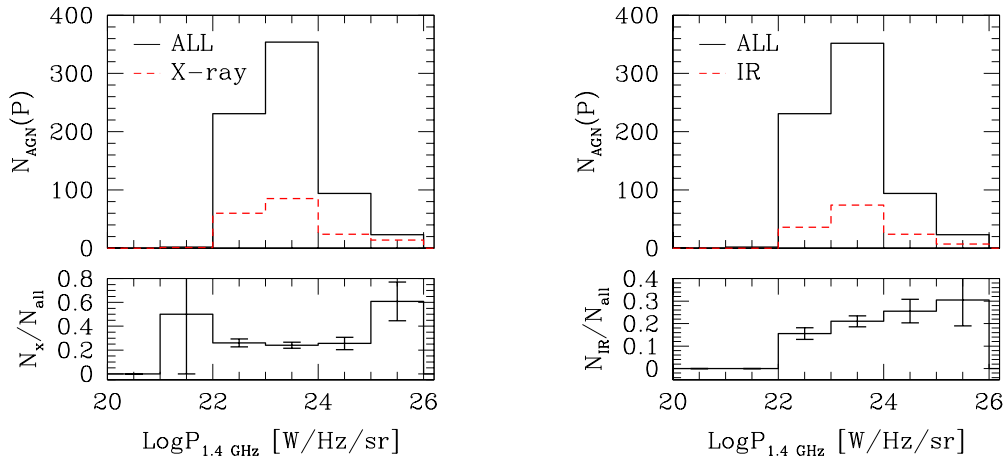


Figure 10. Distribution of radio powers for $F_{1.4\text{GHz}} \geq 0.06$ mJy COSMOS-VLA radio-selected AGNs of different types. The dashed line in the left-hand panel represents sources which are also classified as AGNs in the X-ray, that in the right-hand panel those which present AGN emission in the MIR band. The solid lines are for all radio-selected AGNs. The bottom panels highlight the ratio between the two quantities. Errorbars correspond to 1σ Poissonian estimates.

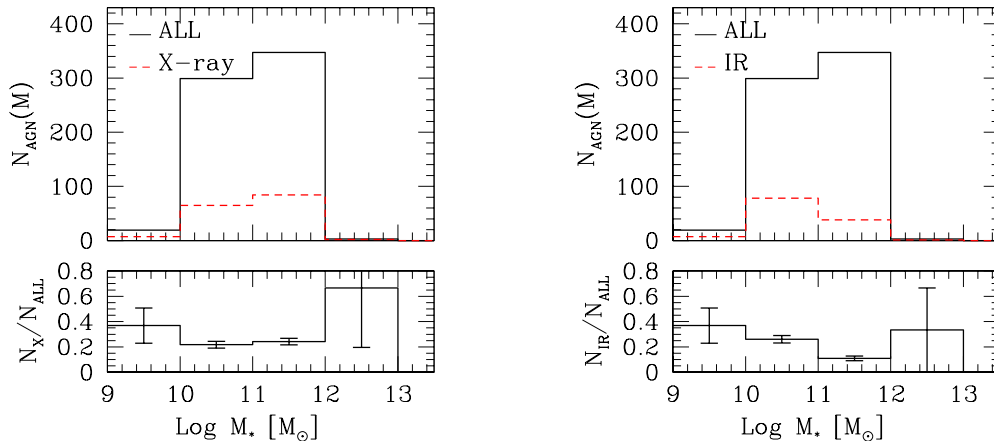


Figure 11. Distribution of stellar masses for $F_{1.4\text{GHz}} \geq 0.06$ mJy COSMOS-VLA radio-selected AGNs of different types. The dashed line in the left-hand panel represents sources which are also classified as AGNs in the X-ray, while that in the right-hand panel those which present AGN emission in the MIR band. The solid lines are for all radio-selected AGNs. The bottom panels highlight the ratio between the two quantities. Errorbars correspond to 1σ Poissonian estimates.

systematically more massive and older than the other class of sources. We can therefore envisage an evolutionary track for radioactive AGNs which associates MIR emission of AGN origin mainly with the early stages of the lifetime of the radio source, when the host galaxy was young and fewer stars were already in place. Note that this also agrees with our finding (confer Table 1) of an enhanced fraction of MIR emitters in radio-selected AGNs which cohabit with intense episodes of stellar formation. On the other hand, X-ray emission in radio-selected AGNs seems to be mainly associated with a later stage of the evolution of these sources, whereby their hosts have built most of their stellar mass and are on average relatively old. This is also true for radio-selected AGNs which only show emission at radio wavelengths, as these two latter classes of sources seem to be indistinguishable from each other.

Amongst the pieces of information which can be gathered from Table 1, we also find that the majority of radio-active AGNs which also emit in the MIR band are associated with FIR activity. Indeed, 83 out of 141 sources (corresponding to 59 percent of the subsample) are detected in the COSMOS-*Herschel* maps, while

only 44 per cent of radio AGNs with emission in the X-ray are instead found to be associated with ongoing star formation within the host galaxy. This finding further confirms the conclusions previously reached: MIR emission is mainly favoured in hosts which are younger than those hosting AGNs which are only active in the radio or in the radio+X-ray bands. Indeed, as clearly shown in Fig. 14 which reports the distributions of FIR luminosities for these two sub-classes of AGNs as compared with the distribution observed for the whole population of radio-selected AGNs which show up in the *Herschel* maps, while the fraction of X-ray AGNs stays constant for increasing FIR luminosities, this is found to monotonically increase in the case of AGNs which also emit in the MIR band.

6 CONCLUSIONS

By making use of the recent catalogue of redshifts produced by Laigle et al. (2016) for galaxies belonging to the COSMOS field, we have performed a thorough analysis of the population of 1.4

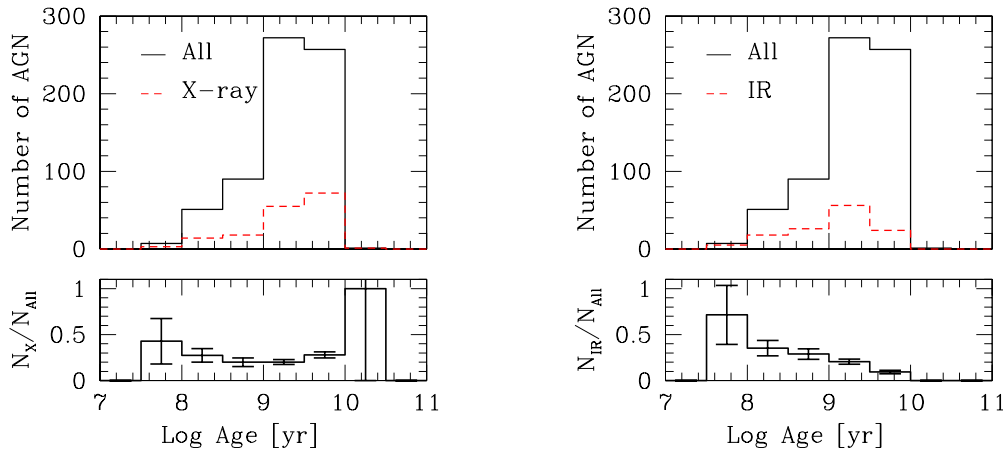


Figure 12. Distribution of ages τ for the hosts of $F_{1.4\text{GHz}} \geq 0.06$ mJy COSMOS-VLA radio-selected AGNs of different types. The dashed line in the left-hand panel represents sources which are also classified as AGNs in the X-ray, while that in the right-hand panel those which present AGN emission in the MIR band. The solid lines are for all radio-selected AGNs. The bottom panels highlight the ratio between the two quantities. Errorbars correspond to 1σ Poissonian estimates.

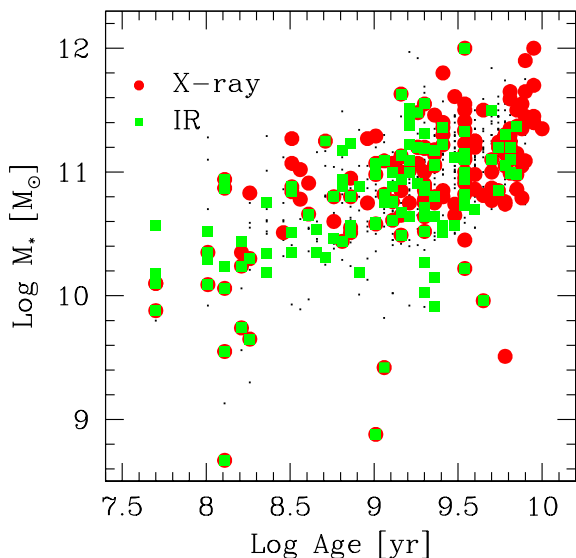


Figure 13. Stellar masses as a function of ages for those galaxies host of a radio-selected AGNs. Filled (red) circles identify AGNs which also emit in the X-ray, while (green) squares represent AGNs which show signs for AGN activity also in the MIR band. The black dots represent the whole parent radio-AGN population.

GHz-selected galaxies on the same COSMOS area and on their FIR properties. This can be considered as a completion of the work presented in Magliocchetti et al. (2014).

About 90 per cent of the sources from the VLA-COSMOS survey (Bondi et al. 2008) are found to have a counterpart in the Laigle et al. (2016) catalogue. These objects have then been sub-divided into radio-active AGNs and radio-emitting star-forming galaxies solely on the basis of their radio luminosity. Out of 2123 radio sources endowed with a redshift estimate, 704 (corresponding to ~ 33 per cent of the parent population) are AGNs and the remaining star-forming galaxies. By then looking for FIR counterparts on the *Herschel*-PEP (Lutz et al. 2011) maps, we found that 272 of such radio-emitting AGNs are also FIR emitters. The redshift distribution of the sub-class of FIR emitters mirrors that of the whole parent

population of radio-active AGNs and features a prominent peak at $z \simeq 1$ and a broad tail which extends up to $z \simeq 4$.

The main conclusions that can be drawn from our analysis can be summarized as follows.

(i) FIR emitters amongst radio-active AGNs are preferentially found at low, $\log P_{1.4\text{GHz}} \lesssim 10^{23}$ [$\text{W Hz}^{-1} \text{sr}^{-1}$], radio luminosities. However, this is only true for $z \lesssim 1$. At higher redshifts, the fraction of FIR emitters of higher radio luminosities increases and by $z \simeq 2$ there is no dependence of such fraction on radio luminosity.

(ii) Similarly, in agreement with the results of Magliocchetti et al. (2014), FIR emitters are found preferentially associated with galaxies of low, $M_* \lesssim 10^{11} M_\odot$, stellar masses only in the local universe. At higher redshifts, such an effect loses its importance, and by $z \simeq 2$ galaxies of all stellar masses have the same chances of hosting an FIR-active, radio-selected AGN.

(iii) Also, the distributions of the ages of the hosts of FIR-active and FIR-quiet AGNs are indistinguishable from each other at redshifts $z \gtrsim 2$. More locally, these two classes of sources evolve differently and by $z \lesssim 1$ FIR-quiet sources are found preferentially associated with older galaxies.

(iv) As it was in Magliocchetti et al. (2014, 2016), we find also in this case that FIR emission is entirely to be attributed to intense episodes of star formation ongoing within the host galaxy. In this work, we have shown that these episodes are so intense that the FIR luminosities of radio-selected AGNs are on average higher than those of star-forming galaxies selected from the same radio sample in a consistent way. Furthermore, the distributions of stellar masses and SFRs for these two classes of sources clearly show that FIR-active radio-selected AGNs are on average not only more FIR-bright, but also more massive than star-forming galaxies. However, once again, this is only true in the local, $z \lesssim 1$, universe. At higher redshifts, the hosts of FIR-bright radio-selected AGNs and star-forming galaxies are indistinguishable from each other.

The picture which therefore emerges from our analysis is that of a substantial similitude amongst galaxies which host a radio-active AGN, independent of whether the AGN phenomenon is associated with concomitant star formation within the host, and also of a similitude between the hosts of radio-selected AGNs and those of radio-selected star-forming galaxies. However, this is only true

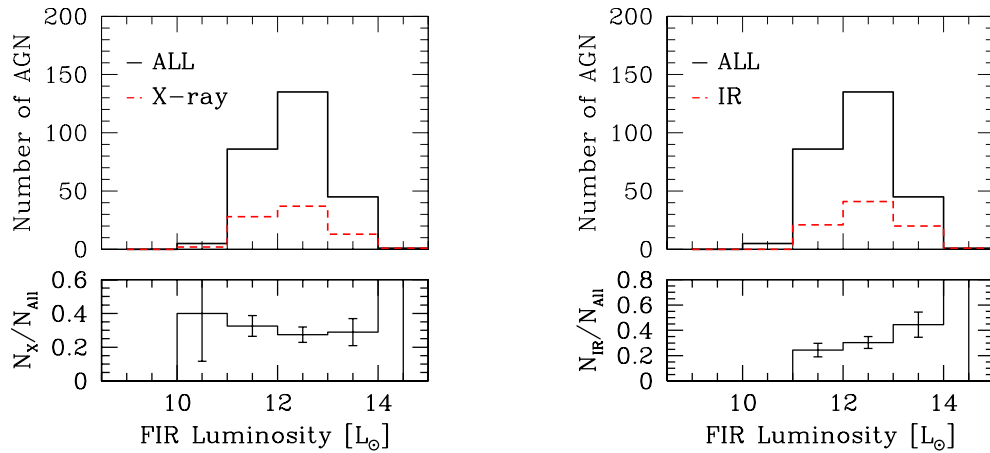


Figure 14. Distribution of FIR luminosities for $F_{1.4\text{GHz}} \geq 0.06$ mJy COSMOS-VLA radio-selected AGNs of different types. The dashed line in the left-hand panel represents sources which are also classified as AGNs in the X-ray, while that in the right-hand panel those which present AGN emission in the MIR band. The solid lines are for all radio-selected AGNs which also present FIR emission. The bottom panels highlight the ratio between the two quantities. Errorbars correspond to 1σ Poissonian estimates.

at high, $z \gtrsim 1-1.5$, redshifts. In the more local universe, these similitudes break down and likewise star-forming galaxies, also radio-selected AGNs associated with FIR emission preferentially inhabit hosts which are smaller and younger than those characterizing the whole radio-active AGN parent population. Furthermore, such galaxies are preferentially occupied by AGNs of relatively low-radio luminosities.

Lastly, we have investigated the properties of radio-selected AGNs which also show signatures for AGN emission at other wavelengths. We find that about 26 per cent of the radio AGNs belonging to our sample also emit in the X-ray, while ~ 20 per cent are also active in the MIR band. Both these percentages rise to ~ 30 per cent in the case of radio-selected AGNs which are also associated with star formation within the host galaxy.

Our results indicate that while the sub-class of X-ray emitting AGNs does not exhibit any sensible difference with respect to the whole radio-selected AGN population, the same is not true for those radio-emitting AGNs which also show signatures for AGN activity in the MIR waveband. In fact, we find that this latter class of sources preferentially inhabits galaxies which are on average younger, less massive and more active at FIR wavelengths than the parent radio-AGN population.

We can therefore envisage an evolutionary track for radio-active AGNs which associates MIR emission mainly with the early stages of the lifetime of the radio source, when the host galaxy was young and not many stars were already in place. On the other hand, X-ray emission in radio-selected AGNs seems to be mainly associated with a later stage of the evolution of these sources, whereby their hosts are relatively old and have already built most of their stellar mass. This is also true for radio-selected AGNs which only show emission at radio wavelengths, as these two latter classes of sources seem to be indistinguishable from each other.

AGNs selected at all wavelengths (radio, X-ray and MIR) should represent objects caught in a short-lived, transition phase, with likely still ongoing star formation, and possibly associated with outflowing winds. Interestingly, in three out of four cases in which ionized outflows have been clearly detected through spatially resolved near-infrared follow-ups of luminous X-ray or MIR-selected AGNs in the COSMOS field (Perna et al. 2015a,b; Brusa et al. 2016), the sources are also revealed as radio-active AGNs, and are indeed part of the sample presented in this work. This observational result therefore

fits a scenario where radiative-driven winds, produced when the black hole is accreting at its maximum, induce shocks in the host galaxy, accelerating relativistic particles which can then emit in the radio band (e.g. Zubovas & King 2012).

ACKNOWLEDGEMENTS

MM and MB wish to thank the DFG Cluster of Excellence ‘Origin and Structure of the Universe’ (www.universe-cluster.de) for partial support during the completion of this work. We also wish to thank the referee for his/her constructive comments which helped improving the paper.

This paper is based on data products from observations made with ESO Telescopes at the La Silla Paranal Observatory under ESO programme ID 179.A-2005 and on data products produced by TERAPIX and the Cambridge Astronomy Survey Unit on behalf of the UltraVISTA consortium.

REFERENCES

- Appleton P. N. et al., 2004, *ApJS*, 154, 147
 Bondi M. et al., 2003, *A&A*, 403, 857
 Bondi M., Ciliegi P., Schinnerer E., Smolcic V., Jahke K., Carilli C., Zamorani G., 2008, *ApJ*, 681, 1135
 Bonzini M. et al., 2012, *ApJS*, 203, 15
 Bonzini M., Padovani P., Mainieri V., Kellermann K. I., Miller N., Rosati P., Tozzi P., Vattakunnel S., 2013, *MNRAS*, 436, 3759
 Bonzini M. et al., 2015, *MNRAS*, 453, 1079
 Boyle B. J., Cornwell T. J., Middleberg E., Norris R. P., Appleton P. N., Smail I., 2007, *MNRAS*, 385, 1143
 Brand K., Rawlings S., Hill G. J., Tufts J. R., 2005, *MNRAS*, 357, 1231
 Brinchmann J., Charlot S., White S. D. M., Tremonti C., Kauffmann G., Heckman T., Brinkman J., 2004, *MNRAS*, 351, 1151
 Brusa M. et al., 2016, *A&A*, 588, A58
 Bruzual G., Charlot S., 2003, *MNRAS*, 344, 1000
 Capak P. et al., 2007, *ApJS*, 172, 99
 Carilli C. L., Furlanetto S., Briggs F., Jarvis M., Rawlings S., Falcke H., 2004, *New Astron. Rev.*, 48, 1029
 Civano F. et al., 2016, *ApJ*, 819, 62
 Chang Y.-Y. et al., 2017, *MNRAS*, 466, L103
 De Breuck C. et al., 2010, *ApJ*, 725, 36
 Del Moro A. et al., 2013, *A&A*, 549, A59
 Donley J. L. et al., 2012, *ApJ*, 748, 142

- Fanaroff B. L., Riley J. M., 1974, *MNRAS*, 167, 31
 Fine S., Shanks T., Nikoloudakis N., Sawangwit U., 2011, *MNRAS*, 418, 2251
 Garn T., Green D. A., Riley J. M., Alexander P., 2009, *MNRAS*, 397, 1101
 Ilbert O. et al., 2010, *ApJ*, 709, 644
 Ilbert O. et al., 2013, *A&A*, 2013, 556, A55
 Johnston S. et al., 2007, *PASA*, 24, 174
 Jonas J. L., 2009, *Proc. IEEE*, 97, 1522
 Kennicutt R. C., Jr, 1998, *ARA&A*, 36, 189
 Laigle C. et al., 2016, *ApJS*, 224, 24
 Leipski C., Antonucci R., Ogle P., Whysong D., 2009, *ApJ*, 701, 891
 Lindsay S. N. et al., 2014a, *MNRAS*, 440, 1527
 Lindsay S. N., Jarvis M. J., McAlpine K., 2014b, *MNRAS*, 2322, 2332
 Lutz D., 2014, *ARA&A*, 52, 373
 Lutz D. et al., 2011, *A&A*, 532, 20
 McAlpine K., Jarvis M. J., Bonfield D. G., 2013, *MNRAS*, 436, 1084
 McCracken H. J. et al., 2012, *A&A*, 544, 156
 Magliocchetti M., Maddox S. J., Wall J. V., Benn C. R., Cotter G., 2000, *MNRAS*, 318, 1047
 Magliocchetti M., Porciani C., 2003, *MNRAS*, 346, 186
 Magliocchetti M. et al. (the 2dFGRS Team), 2002, *MNRAS*, 333, 100
 Magliocchetti M. et al. (the 2dFGRS Team), 2004, *MNRAS*, 350, 1485
 Magliocchetti M., Andreani P., Zwaan M. A., 2008, *MNRAS*, 383, 479
 Magliocchetti M. et al., 2014, *MNRAS*, 442, 682
 Magliocchetti M., Lutz D., Santini P., Salvato M., Popesso P., Berta S., Pozzi F., 2016, *MNRAS*, 456, 431
 Magliocchetti M., Popesso P., Brusa M., Salvato M., Laigle C., McCracken H. J., Ilbert O., 2017, *MNRAS*, 464, 3271
 Mao M. Y. et al., 2011, *ApJ*, 731, 79
 Marchesi S. et al., 2016, *ApJ*, 817, 34
 Mauch T., Sadler E. M., 2007, *MNRAS*, 375, 931
 Morrison G. E., Owen F. N., Dickinson M., Ivison R. J., Ibar E., 2010, *ApJS*, 188, 178
 Norberg P. et al., 2002, *MNRAS*, 332, 827
 Norris R. P. et al., 2011, *ApJ*, 736, 55
 Padovani P., Bonzini M., Kellermann K., Mainieri V., Miller N., Tozzi P., 2015, *MNRAS*, 452, 1263
 Peng Y. j. et al., 2010, *ApJ*, 721, 193
 Perna M. et al., 2015a, *A&A*, 574, A82
 Perna M. et al., 2015b, *A&A*, 583, A72
 Pilbratt G. et al., 2010, *A&A*, 518, L1
 Poglitsch A. et al., 2010, *A&A*, 518, L2
 Porciani C., Magliocchetti M., Norberg P., 2004, *MNRAS*, 355, 1010
 Prandoni I., Gregorini L., Parma P., de Ruiter H. R., Vettolani G., Zanichelli A., Wieringa M. H., Ekers R. D., 2001, *A&A*, 369, 787
 Retana-Montenegro E., Roettgering H. J. A., 2017, *A&A*, 600, 97
 Rodighiero G. et al., 2011, *ApJ*, 739, L40
 Salpeter E. E., 1955, *ApJ*, 121, 161
 Schinnerer E. et al., 2004, *AJ*, 128, 1974
 Schinnerer E. et al., 2007, *ApJS*, 172, 46
 Schinnerer E. et al., 2010, *ApJS*, 188, 384
 Scoville N. et al., 2007, *ApJS*, 172, 1
 Seymour N. et al., 2011, *MNRAS*, 413, 1777
 Simpson C. et al., 2012, *MNRAS*, 421, 3060
 Smolcic V. et al., 2017, *A&A*, 602, A2
 Taniguchi Y. et al., 2007, *ApJS*, 172, 9
 Wake D. A., Croom S. M., Sadler E. M., Johnston H. M., 2008, *MNRAS*, 391, 1674
 White S. V., Jarvis M. J., Haussler B., Maddox N., 2015, *MNRAS*, 448, 2665
 Zehavi I. et al., 2005, *ApJ*, 630, 1
 Zubovas K., King A., 2012, *ApJ*, 745, L34

APPENDIX

This appendix is devoted to the discussion of the level of contamination of the AGN sample considered in this work and will be

divided into two parts: (1) contamination due to the population of star-forming galaxies and (2) contamination due to AGNs which owe their radio emission to star-forming activity rather than to the AGN itself.

(1) *Contamination from star-forming galaxies.* One possible source of contamination is due to the unremoved presence of star-forming galaxies of radio luminosities higher than P_{cross} within the AGN sample. In order to assess the importance of such an effect, we have estimated the fraction of star-forming galaxies within our sample of radio-selected sources according to the radio luminosity function of McAlpine, Jarvis & Bonfield (2013). Results at the various redshifts are presented in Fig. A1, where the vertical dashed lines represent the values of $P_{\text{cross}}(z)$ as defined in Section 3. As it is possible to notice, in all cases star-forming galaxies tend to disappear very rapidly beyond P_{cross} . In more detail, in the local universe ($z = 0$ and $z = 0.5$ panels), the fraction of star-forming galaxies is ~ 28 per cent at P_{cross} , while at $2 \times P_{\text{cross}}$ this is already as low as ~ 10 per cent. At redshift $z = 1$, instead we find $N_{\text{SF}}/N_{\text{TOT}} \simeq 20$ per cent at P_{cross} and ~ 6 per cent at $2 \times P_{\text{cross}}$, while in the more distant, $z \geq 1.5$, universe we have that the fraction of contaminants is about 10 per cent at P_{cross} , and between 2 and 4 per cent at $2 \times P_{\text{cross}}$.

The above results clearly show that star-forming galaxies constitute a negligible fraction of the sample of radio-selected AGNs already at radio luminosities which are twice as bright as the chosen threshold. In order to assess the robustness of the results presented throughout this paper, we have then performed once again our analysis by only including sources with $P > 2 \times P_{\text{cross}}$ (444 sources instead of 704, confer Section 3). As an example, the results for what concerns the distribution of AGNs which are also active in the FIR bands as a function of radio luminosity (left-hand panel), stellar mass of the host (middle panel) and age of the host (right-hand panel) are presented in Fig. A2, whereby the filled histograms reproduce the results already presented in Section 3 (Figs 2–4), while the dashed ones what is obtained if we only concentrate on sources brighter than twice the luminosity threshold P_{cross} . As it is clear from the figure, there is no appreciable difference between

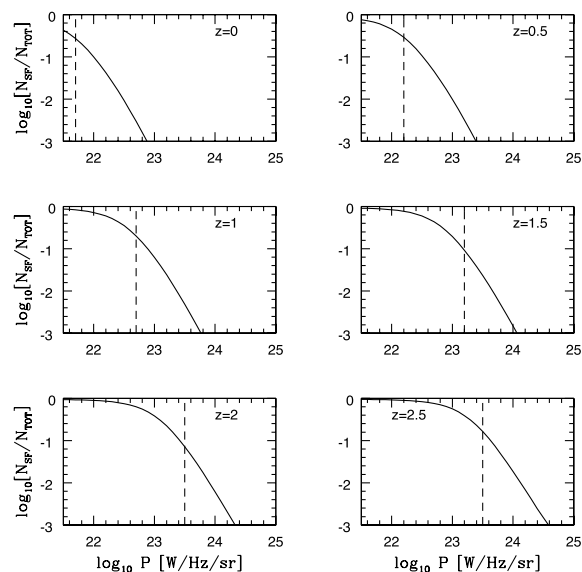


Figure A1. Fraction of star-forming galaxies as a function of radio luminosity as derived from the luminosity function of McAlpine, Jarvis & Bonfield (2013). The various panels represent different redshift intervals.

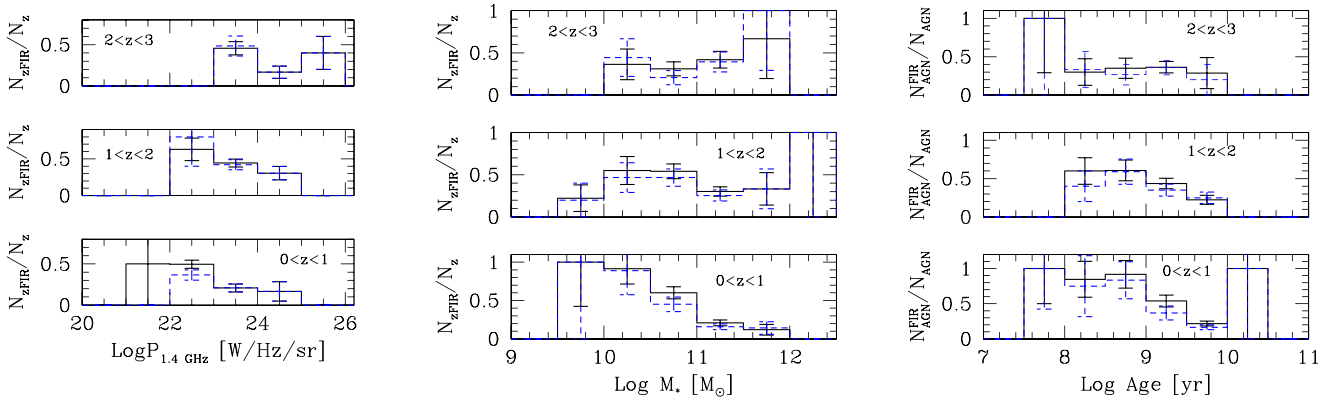


Figure A2. Fraction of radio-selected AGNs which also emit in the FIR bands as a function of (1) radio luminosity (left-hand panel), (2) stellar mass of the host (middle panel) and (3) age of the host (right-hand panel). The distributions are presented in three redshift ranges. In all cases, the filled histograms reproduce the results already presented in Section 3, while the dashed ones show the variations obtained if one only considers sources brighter than twice the luminosity threshold P_{cross} .

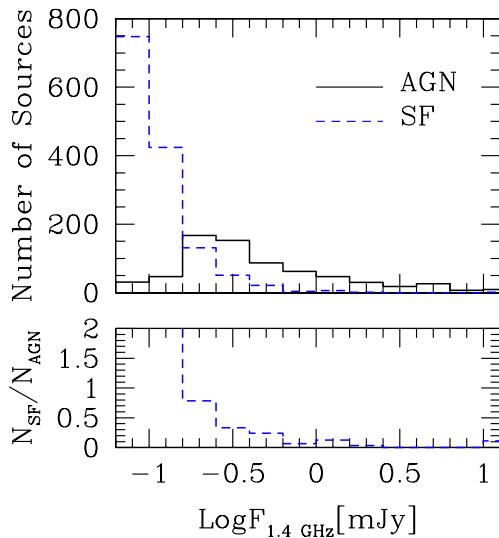


Figure A3. Flux distribution of radio-emitting AGNs (filled histogram) and radio-emitting star-forming galaxies (dashed histogram) selected by the method highlighted in Section 3. The bottom panel represents the ratio between these two quantities.

the distributions of these two samples. In other words, the eventual presence of unremoved star-forming galaxies in the proximity of P_{cross} does not affect these or any other behaviour or conclusion of this work and also of the previous ones belonging to the same series (Magliocchetti et al. 2014; Magliocchetti et al. 2016).

(2) *Contamination from radio-quiet AGNs.* Another source of concern is represented by the possibility of contamination of our sample due to radio-quiet AGNs which emit in the radio waveband only thanks to star-forming activity within the host galaxy. This issue was already discussed in Magliocchetti et al. (2014) who concluded that chances for such a contamination were extremely low. To further extend this point, we have computed the radio flux distribution for the two populations of radio-emitting AGNs and star-forming galaxies as obtained by applying the method described in Section 3. This is shown in Fig. A3, which clearly indicates that radio-selected AGNs start appearing in the COSMOS sample at fluxes $F_{1.4\text{GHz}} \gtrsim 0.15$ mJy and become the dominant population

above $F_{1.4\text{GHz}} \simeq 0.5$ mJy. This result is in perfect agreement not only with all those found in the literature, but also with the recent ones presented by Padovani et al. (2015), which are based on the selection method of Bonzini et al. (2015) and with those presented in Smolcic et al. (2017). Indeed, in agreement with our findings, fig. 1 of Padovani et al. (2015, but also confer figs 12 and 13 of Smolcic et al. 2017) clearly shows that radio-emitting AGNs (or what Padovani et al. 2015 call ‘radio-loud AGNs’ and Smolcic et al. 2017 call ‘radio-excess’ sources; names vary but the concept is the same: radio-detected AGNs which owe their emission to accretion processes rather than to star formation within the host galaxy) beyond $F_{1.4\text{GHz}} \simeq 0.5$ mJy are between 10 and 20 times more numerous than the other classes of sources. Fig. 1 of Padovani et al. (2015) also shows (in agreement with, e.g. the results of White et al. 2015) that beyond $F_{1.4\text{GHz}} \simeq 0.15$ mJy the contribution to the total number counts of the population of radio-quiet AGNs is also negligible. This means that the chances that our AGN sample is contaminated by AGNs which owe their emission to star-forming processes rather than accretion are negligible.

In this respect, we would also like to point out the very recent results presented in Magliocchetti et al. (2017), which show that the clustering properties of radio-selected AGNs within the COSMOS area (i.e. basically the same sample presented in this paper) are in full agreement with all those found in the literature (e.g. Magliocchetti et al. 2004; Brand et al. 2005; Wake et al. 2008; Fine et al. 2011; Lindsay et al. 2014; Lindsay, Jarvis & McAlpine 2014b; Retana-Montenegro & Roettgering 2017). This would not be possible if some different population had sensibly contaminated the sample, since the clustering lengths of radio-quiet AGNs (e.g. Porciani, Magliocchetti & Norberg 2004; Retana-Montenegro & Roettgering 2017) and star-forming galaxies (e.g. Norberg et al. 2002; Magliocchetti & Porciani 2003; Zehavi et al. 2005) are much smaller than those normally measured for radio-loud AGNs and contamination would have brought the measured clustering signal below that which is typical of the radio-loud AGN population.

This paper has been typeset from a $\text{\TeX}/\text{\LaTeX}$ file prepared by the author.